Submitted, accepted and published by
Energy & Fuels 2007, 21, 1843-1853

Reduction Kinetics of Cu-, Ni-, and Fe-based Oxygen Carriers Using Syngas ($CO+H_2$) for Chemical-Looping Combustion

Alberto Abad [*], *Francisco García-Labiano, Luis F. de Diego, Pilar Gayán, Juan Adánez*

Instituto de Carboquímica (CSIC), Department of Energy and Environment, Miguel Luesma Castán 4, Zaragoza 50018, Spain

Author e-mail address: abad@icb.csic.es

Abstract

The reactivity of three Cu-, Fe-, and Ni-based oxygen carriers to be used in a chemical-looping combustion (CLC) system using syngas as fuel has been analyzed. The oxygen carriers exhibited high reactivity during reduction with fuel gases present in syngas (H_2 and CO), with average values in the range 8-30 % min^{-1}. No effect of the gas products (H_2O, CO_2) on the reduction reaction rate was detected. The kinetic parameters of reaction with H_2 and CO have been determined by thermogravimetric analysis. The grain model with spherical or plate-like geometry in the grain was used for the kinetic determination, in which the chemical reaction controlled the global reaction rate. The

[*] Corresponding author. Tel: +34976 733977. Fax: +46976 733318. E-mail: abad@icb.csic.es

activation energies determined for these reactions were low, with values ranging from 14 to 33 kJ mol^{-1}. The reaction order depended on the reacting gas, and values from 0.5 to 1 were found. Moreover, the reactivity of the oxygen carriers when both H_2 and CO are simultaneously present in the reacting gases has been analyzed, both at atmospheric and pressurized conditions. For the Cu- and Fe-based oxygen carriers, the reaction rate of the oxygen carrier with syngas corresponded to the addition of the reaction rates for the individual fuel gases, H_2 and CO. For the Ni-based oxygen carrier the reaction rate was that corresponding to the fuel gas that reacted faster with the oxygen carrier at the reacting conditions (fuel concentration, temperature and pressure). The consequences of the behaviour of the reaction of syngas and the water-gas shift (WGS) equilibrium on the design of the fuel reactor of a CLC system have been analyzed. A preliminary estimation of the solids inventory for the use of syngas in the fuel reactor of a CLC system gave values in the range of 19-34 kg MW^{-1} when the WGS equilibrium was considered be instantaneous.

Keywords: Chemical-Looping Combustion, Oxygen carrier, Kinetics, Syngas.

Introduction

The possible linkage between rising levels of atmospheric carbon dioxide and global warming has led to international agreements to reduce carbon dioxide emissions. The main contributor to increasing atmospheric CO_2 concentration is fossil fuel combustion for power generation, transport, industry, and domestic use. About a third of the global CO_2 emissions comes from combustion of fossil fuels in power generation.[1] CO_2 capture and storage has been identified as the best mitigation action to reduce the CO_2 emissions from power plants, and still using fossil fuels. Other mitigation options include

energy efficiency improvements, to switch to less carbon-intensive fuels, the use of nuclear power, renewable energy sources, or enhancement of biological sinks.

There are different technologies available or currently under development which accomplish the capture of CO_2 from combustion sources, i.e., pre-combustion, post-combustion or oxyfuel technologies.[1-3] Nowadays, most of these technologies have high energy penalty for the CO_2 capture and result in an increase in the cost of energy production. In this sense, chemical-looping combustion (CLC) offers a high potential to reduce the cost associated with CO_2 separation.[1,4] The use of coal in power plants with low energy penalty for CO_2 capture can be accomplished by a process integrating coal gasification and chemical-looping combustion (CLC).[5,6] In this process, the syngas produced from coal gasification is used as fuel in a CLC system for power generation with CO_2 capture. Simulations made by Jin and Ishida[6] and Wolf et al.[7] showed that this process have the potential to achieve an efficiency of about 5-10% points higher than a similar combined cycle that uses conventional CO_2 capture technology. To get the benefits in the energetic efficiency the CLC system must operate at pressurized conditions and at high temperature, e.g. 1-2 MPa and 1400-1500 K.

CLC is a two-step gas combustion process based on the transfer of oxygen from the combustion air to the fuel by means of an oxygen carrier in the form of a metal oxide. The fuel, natural gas or synthesis gas from coal gasification, is not mixed with air, and produces a pure CO_2 stream without extra energy requirements. The system is composed of two reactors, the air and fuel reactors, as shown in Figure 1. The fuel gas is introduced to the fuel reactor (FR), where it is oxidized by the oxygen carrier. At full conversion of the fuel gas, the exit gas stream from the fuel reactor contains CO_2 and H_2O, and almost pure CO_2 can be easily collected for subsequent use, i.e. compression and storage, after H_2O condensation. The particles of the oxygen carrier are transferred to the air reactor (AR) where they are regenerated by taking up oxygen from the air. The exit gas stream from the air reactor contains N_2 and some unused O_2. The total amount of heat evolved from reactions in the two reactors is the same as for

normal combustion, where the oxygen is in direct contact with fuel. Since the process requires a good contact between gas and solids as well as a flow of solid material between the fuel and air reactors, the use of two interconnected fluidized beds have advantages over other designs.[8]

The key issue in the CLC system performance is the oxygen carrier material. Iron-, nickel-, and copper-based oxygen carriers have been selected as the most promising materials to be used in a CLC process. In general, the metal oxide is combined with an inert which acts as a porous support providing a higher surface area for reaction, as a binder for increasing the mechanical strength and attrition resistance. There are several works about the behaviour of these type of oxygen carriers with H_2 at atmospheric[9-18] and pressurized conditions.[19-21] However, less work concerning the reactivity for CO[16,17] or syngas have been done.[6,15,22] In general, higher reactivity for syngas components with respect to reactivity for methane were found. In these works, different kind of oxygen carriers were identified as possible materials to be used in a CLC system, in basis to high enough reactivity and durability with the number of reduction-oxidation cycles, and no presence of agglomeration in a fluidized bed.

The use of syngas in a CLC system has been successfully accomplished in a 300 W continuously operated reactor for Mn-, Ni-, and Fe-based oxygen carriers.[23-25] For the scale-up it is necessary to know both the type of oxygen carrier and its reaction kinetics with respect to the different fuel gases (H_2 and CO) and oxygen, because these data will affect to the design (i.e., hydrodynamic behavior, residence time or solids inventory) and optimization of the CLC plant.[17] On the other hand, during the methane combustion in a CLC system, CO and H_2 can appear throughout side reactions and react with the oxygen carrier, especially with Ni-based oxygen carriers. Moreover, CO and H_2 can appear as intermediate products during combustion of solid fuels, e.g. coal, in a CLC system.[26] Therefore, it is also of practical interest to know the reactivity of the oxygen carriers with CO and H_2 for the development of CLC using solid fuels or natural gas as fuel.

There are very few works in the literature related with the determination of kinetic parameters for the reaction of oxygen carriers with syngas components, H_2 and CO. Ishida et al.[10] used an unreacted-core model (UCM) at the whole particle to interpret their experimental results in the reduction reactions of Ni-based oxygen carriers with H_2. The reduction reaction was controlled by the chemical reaction resistance, and an activation energy of 82 kJ mol^{-1} was found. García-Labiano et al.[16] used an UCM for plate-like geometry to describe the reduction reaction with H_2 and CO for a copper oxide impregnated on alumina oxygen carrier. The activation energy for H_2 was 33 kJ mol^{-1} and for CO was 14 kJ mol^{-1}. Reactions order of 0.6 and 0.8 were found for H_2 and CO, respectively. Because of the advantages of the use of a pressurized system, the reaction kinetic of CO and H_2 at pressurized conditions should be determined. The effect of total pressure on the reaction rate of the oxygen carriers with H_2 and CO was analysed in a previous work.[21] The experiments showed that an increase in total pressure did not cause the expected increase in the reaction rate by the increase in the partial pressure of the reacting gas; even in some cases, the reaction rate decreased increasing the total pressure. It was concluded that the kinetic parameters necessary to design pressurized CLC systems must be determined at the operating pressure of the industrial plant. However, there is not any work about the implications that the individual reactivity with H_2 and CO has on the behaviour of the fuel reactor when syngas is used.

The objective of this work was to investigate the reactivity of three oxygen carriers based on copper, nickel and iron with syngas ($CO+H_2$) at atmospheric and pressurized conditions. The reactivity of the oxygen carriers with syngas was analyzed based on individual reactivities with H_2 and CO. The effect of temperature, gas concentration, and reaction gas products (CO_2 and H_2O) was examined. From the results obtained, implications in the behaviour of the fuel reactor of a CLC system were deduced.

Experimental Section

Materials. Three oxygen carriers using Al_2O_3 as support were used in this work: particles of copper (II) oxide prepared by impregnation (Aldrich Chemical Company), and nickel- and iron-based particles prepared by freeze-granulation at Chalmers University of Technology.[27] The samples were designated as Cu10Al-I, Ni40Al-FG, and Fe60Al-FG. The samples were characterized by Hg porosimetry, and N_2 physisorption to determine the internal structure of the particles. Table 1 shows the main physical characteristics of the materials, as well as their oxygen transport capacity. The oxygen transport capacity was defined as $R_{OC}=(m_{ox}-m_{red})/m_{ox}$, where m_{ox} and m_{red} are the masses of the oxygen carrier in the oxidised and reduced form, respectively. The oxygen transfer capacity of the oxygen carriers depends both on the active metal oxide content, and on the type of metal oxide considered. In this sense, the oxygen transport capacity for pure metal oxides, R_o, is higher for NiO/Ni (0.21) and CuO/Cu (0.20), than for Fe_2O_3/Fe_3O_4 (0.03). When the content of metal oxide in the oxygen carrier is considered, the oxygen transport capacity, R_{OC}, for Cu10Al-I is lower than this for Fe60Al-FG because of their lower metal oxide content, see Table 1.

TGA experimental set-up. The reactivity experiments were performed in CI Electronics Ltd and Cahn TG-2151 type thermogravimetric analyzers, working at atmospheric and pressurised conditions, respectively. More details of these apparatus can be found elsewhere.[16,21]

Procedure. The experiments at atmospheric pressure were carried out in the CI Electronics Ltd thermobalance system. The oxygen carrier sample (30-70 mg) was loaded in the sample-holder and introduced into the reactor. The sample-holder was a wire mesh platinum basket (14 mm diameter and 8 mm height) to reduce mass transfer resistance around the sample. Indeed, to avoid the contact between the particles and to minimize the interparticle mass transfer resistance, the sample was loaded between layers of quartz wool. The oxygen carriers were heated to the desired temperature in an air atmosphere. Once the set temperature was reached, the experiment was started by exposing the oxygen

carrier to alternating reducing and oxidizing conditions. The reacting gas mixture (6 cm^3 s^{-1} STP) was measured and controlled by electronic mass flow controllers. When water was introduced, the reacting gas was bubbling through a saturator containing water at a selected temperature necessary to reach the desired water concentration in the reacting stream. To avoid the mixing of fuel gas and air, nitrogen was introduced for two minutes after each reducing and oxidizing period. Five cycles of reduction and oxidation were carried out for each experimental condition. The sample normally stabilized after the first reduction cycle, which it was slower compared to following cycles. In this work, the oxygen carrier reactivity corresponding to the fifth cycle was used to determine the kinetic parameters.

The experiments at higher pressures were carried out in a pressurized thermogravimetric analyzer (PTGA), Cahn TG-2151 type. The procedure was similar to the above described for atmospheric conditions, but including a pressurization step prior to starting the reduction and oxidation cycles.

Kinetic determination for reduction with H_2 or CO. To determine the reaction kinetics of the oxygen carriers with hydrogen the reacting gas was composed by H_2 and H_2O at the desired composition, whereas for the kinetic determination with CO the reacting gas was composed by CO and CO_2. CO_2 was introduced together with CO to avoid carbon formation by the Boudouard reaction. In both cases, nitrogen was used to balance. The composition of the gas was varied to cover the great majority of the gas concentrations present in the fluidized bed fuel reactor of a CLC system (Fuel gas: 5-70 vol%; H_2O: 0-48 vol%; CO_2: 0-40 vol%). The temperature range was varied from 873 to 1223 K for the Fe60Al-FG and Ni40Al-FG oxygen carriers and from 723 to 1073 K for the Cu10Al-FG. For the copper-based oxygen carrier, the temperature was limited to 1073 K to avoid the decomposition of the CuO to Cu_2O in N_2 atmosphere during the inert period between the oxidation and the reduction. To determine the reduction kinetic over the same reacting compound, the sample was always oxidized in the previous step at 1223 K in air, except for the Cu10Al-FG, which was oxidized at 1073 K.

The effect of total pressure on the reactivity of these oxygen carriers with H_2 and CO was determined in a previous work.[21] Total pressure was varied from 0.1 to 3.0 MPa. Two kinds of experiments were carried out, either at constant partial pressure or at constant volume fraction of the fuel gas.

Reactivity with both H_2 and CO in the reacting gas. To determine the reactivity of the oxygen carriers when both H_2 and CO are present in the fuel gas, several experiments were carried out with the presence of both gases in the reacting gas. The experiments were conducted both at atmospheric pressure and at 2 MPa. For the atmospheric experiments, the temperature was 1223 K for the Fe60Al-FG and Ni40Al-FG oxygen carriers and 1073 K for the Cu10Al-FG. The reacting gas was composed by H_2, CO, H_2O and CO_2. The experimental conditions were chosen to minimize the formation of carbon from the reacting gases.[6,12,22] Table 2 shows the gas concentration used in these experiments. H_2O and CO_2 were introduced in the concentrations determined by the water-gas shift (WGS) equilibrium at the reacting temperature, given by the following equation

$$CO + H_2O \rightleftharpoons CO_2 + H_2 \quad (1)$$

As the reaction rate varies with the gas concentration, the concentrations of fuel gases were selected to analyze three different conditions: (c1) the reaction rate with H_2 was higher than that with CO; (c2) the reaction rate with H_2 and CO are similar; and (c3) the reaction rate with H_2 was lower than that with CO. The gas concentrations used at c1, c2 and c3 conditions was selected from the results obtained in the previous section, where the reactivity with H_2 and CO was analyzed separately.

The experiments at 2 MPa were conducted at 1073 K in the PTGA. In this case, it was not possible to feed H_2O into the system. The inlet gas composition was 15 vol% H_2, 5 vol% CO and 10 vol% CO_2. The gas composition at the reacting zone assuming the WGS equilibrium was 10 vol% H_2, 10 vol% CO, 5 vol% CO_2 and 5 vol% H_2O.

Data evaluation. The reduction reaction with H_2 or CO of an oxygen carrier per mol of fuel gas is given by the following equations

$$b\ \mathrm{MeO} + \mathrm{CO} \rightleftharpoons a\ \mathrm{Me} + \mathrm{CO_2} \quad (2)$$

$$b\ \mathrm{MeO} + \mathrm{H_2} \rightleftharpoons a\ \mathrm{Me} + \mathrm{H_2O} \quad (3)$$

where MeO represents the metal oxide (i.e., CuO, NiO or Fe_2O_3), and Me represents a metal or a reduced form of MeO (i.e., Cu, Ni, Fe_3O_4 or FeO). Table 3 shows the values of the stoichiometric parameter *b*, used later in the kinetic model, for the different oxygen carriers and reactions. As later is discussed, the reduced form for Fe60Al-FG oxygen carrier was the iron aluminate, $FeAl_2O_4$. The conversion level of the oxygen carrier for the reduction reaction was calculated as:

$$X_r = \frac{m_{ox} - m}{m_{ox}\, R_{OC}} \quad (4)$$

The oxygen transport capacity of the oxygen carriers, R_{OC}, used in this work is given in Table 1. In the case of Ni40Al-FG, part of the metal oxide used in the preparation (60% NiO) reacted with the support to give aluminates, which are not active for reaction. In this case, the active NiO content of the oxygen carrier was 40%.

Iron compounds needs special attention due to their different final oxidation states during reduction reaction (Fe_2O_3-Fe_3O_4-FeO-Fe). Depending on the ratio H_2O/H_2 or CO_2/CO, the reduction of Fe_2O_3 can finish in one of the above products, and consequently, the value of R_{OC} will be very different depending on the reaction considered. Figure 2 shows the iron compound at equilibrium depending on the ratio between product and reacting gases at 1223 K according to data from Jerndal et al.[28] The gas composition in equilibrium with Fe_3O_4 is region A, with FeO is region B, and with Fe is region C. In the reactivity experiments, different H_2O/H_2 and CO_2/CO ratios were used. The final product for each condition (Fe, FeO or Fe_3O_4) was determined by thermogravimetric analysis. As an example, Figure 3 shows the mass loss, defined as $\omega=m/m_{ox}$, obtained with H_2O/H_2 ratio values of 10, 0.75 and 0.25, corresponding with regions A, B, and C in Figure 2. For H_2O/H_2 ratios of 0.25 and 0.75, the reaction proceeds until the formation of Fe and FeO respectively, corresponding with regions C and B in Figure

2. However, the oxygen carrier never got full conversion during TGA reductions of 20 minutes. For H_2O/H_2 = 0.25, two steps during the reduction reaction were observed. A fast decrease in the mass of sample was observed during the first seconds. Later, the reduction proceed slower, corresponding to the reduction from FeO to Fe, and longer time should be needed to reach full conversion to Fe. For H_2O/H_2 = 0.75, the final conversion was between those for reduction to Fe_3O_4 and FeO. For $H_2O/H_2 \approx 10$ the reduction should proceed only to Fe_3O_4. However, the mass loss observed was higher than that corresponding with Fe_3O_4, and it was similar to the obtained for H_2O/H_2 = 0.75 (see Figure 3). The behavior above showed with H_2O/H_2 ratios of 10, 0.75 and 0.25 is extensive to the rest of conditions: Figure 2 shows that using H_2O/H_2 ratios lower than 0.66 the reduction proceeds towards Fe; however, experimental work using H_2O/H_2 ratios higher than 0.66 the reduction proceeds towards FeO, even with H_2O/H_2 ratios higher than 2.8, corresponding with the region where the reduction should be only to Fe_3O_4.

The above results could be explained because the reduction of Fe_2O_3 does not follow the sequence Fe_2O_3-Fe_3O_4-FeO-Fe. According to Patrick et al.[29], the sequence in the reduction for particles composed by Fe_2O_3 and Al_2O_3 is Fe_2O_3-Fe_3O_4-$FeAl_2O_4$-Fe. Thermodynamic calculations show than $FeAl_2O_4$ is formed at H_2O/H_2 ratios ranging from 0.01 to 365000 at 1223 K, which practically cover all the area of regions A, B and C in Figure 2. At these conditions, the only stable compound is $FeAl_2O_4$. However, in the Fe60Al-FG oxygen carrier there are an excess of Fe_2O_3 (65.7 mol% as FeO) with respect to Al_2O_3 (34.3 mol% as Al_2O_3) to form $FeAl_2O_4$. The Fe in excess (31.4 mol% as FeO) remained as Fe_3O_4 Thus, for ratios higher than 0.66 at 1223 K the final products are a mixture of Fe_3O_4 and $FeAl_2O_4$. For lower H_2O/H_2 ratios, Fe is formed from the Fe_3O_4 reduction, and the final products are a mixture of Fe and $FeAl_2O_4$. For the oxygen carrier Fe60Al-FG the Fe_2O_3/Al_2O_3 molar ratio is 0.96. The mass loss corresponding with all Al_2O_3 in the $FeAl_2O_4$ form, and the rest of Fe as Fe_3O_4 is ω = 0.96, which agrees with the mass loss observed experimentally, see Figure 3. In all experiments, subsequent oxidation with

oxygen showed complete regeneration of the oxygen carrier to Fe_2O_3, indicating that the $FeAl_2O_4$ is an active phase during reduction-oxidation cycles. Similar results to that obtained with H_2 were obtained when using CO at different CO_2/CO ratios.

Thermodynamic calculations show that using iron-based oxygen carriers supported on alumina it is possible to reach full combustion of H_2 and CO into H_2O and CO_2 when Fe_3O_4 and/or $FeAl_2O_4$ are formed. Further reduction to wustite (FeO) or Fe would produce a high decrease in the CO_2 purity obtained in the fuel reactor because of the increase in the equilibrium concentrations of CO and H_2.[28] Therefore, the Fe_2O_3 should be reduced as maximum to a mixture of Fe_3O_4 and $FeAl_2O_4$ in order to get full fuel gas combustion in a CLC system, as it is showed in Figure 3 for Fe60Al-FG in the value ω = 0.96. This value corresponds to the data for R_{OC} = 0.04 showed in Table 1. For kinetic parameters determination, the majority of the experimental work was done at conditions which the reduction reaction stopped at a value of ω = 0.96. However, in some experiments carried out in the TGA it was not possible to stop the reaction in the Fe_3O_4+$FeAl_2O_4$ product, and subsequent reduction happened towards Fe. In these cases, only the first part of the experimental curves, in the range ω = 1-0.96, was used to determine the reaction kinetic.

Kinetic model. There are several resistances that can affect the reaction rate of the oxygen carrier with the fuel gas, e.g. external and internal mass transfer or superficial chemical reaction. Initially, to establish whether external film mass transfer and/or interparticle diffusion were affecting the reaction rate, the gas flow rate and the sample weight were varied in the range 4-6 $cm^3\ s^{-1}$ STP and from 20-80 mg, respectively. It was observed that the reaction rate was not affected by the amount of sample used or the flow rate, indicating that external and inter-particle diffusion was not of importance. Moreover, several experiments showed that particle sizes in the range 90-250 μm did not affect the reaction rates. The experiemental results agreed with previous calculations where we find external and internal mass transfer resistances were not important in the experimental conditions used in this work, and the

reaction is likely chemical reaction determining.[30] For kinetic determination, two different geometries were considered taking into account the structural differences of the oxygen carriers. Fe- and Ni-based oxygen carriers prepared by freeze-granulation exhibited a granular structure, and the shrinking core model (SCM) for spherical grains was considered. The SCM for plate-like geometry in the porous surface of the particle was considered for the Cu-based oxygen carrier prepared by impregnation assuming a uniform layer of metal oxide inside the pores covering the inert material. The equations that describe these models under chemical reaction control in the grain are the following:[31]

for spherical grain geometry

$$\frac{t}{\tau} = 1-(1-X_r)^{1/3} \qquad \tau = \frac{\rho_m\, r_g}{bk\left(C^n - C_{eq}^n\right)} \tag{5}$$

for plate-like geometry

$$\frac{t}{\tau} = X_r \qquad \tau = \frac{\rho_m\, L}{bkC^n} \tag{6}$$

where the kinetic constant follows an Arrhenius type dependence with temperature

$$k = k_0\, e^{-E/R_g T} \tag{7}$$

Equation 5 considers the thermodynamic equilibrium for the reactant gas that occurs in the Ni-based oxygen carriers. For the other metal oxides the value of C_{eq} is zero.

The reactivity of the oxygen carrier, defined as dX_r/dt, was obtained by derivation of equations 5 and 6:

for spherical grain geometry

$$\frac{dX_r}{dt} = \frac{3}{\tau}(1-X_r)^{2/3} \tag{8}$$

for plate-like geometry

$$\frac{dX_r}{dt} = \frac{1}{\tau} \tag{9}$$

The grain radius of the freeze-granulated particles was calculated from porosity and specific surface area measurements (see Table 1) as

$$r_g = \frac{3}{S_{BET}\rho_s} \tag{10}$$

The thickness of the layer of CuO, *L*, over the Al_2O_3 support was determined considering the ASA obtained by H_2 chemisorption and the weight fraction of active CuO in the oxygen carrier particles.

The effect of total pressure on the reaction rate of the oxygen carriers with H_2 and CO was analysed in a previous work.[21] The experiments showed that an increase in total pressure had a negative effect on the reaction rate of all oxygen carriers and reactions. The use of the kinetic rate constant obtained at atmospheric pressure was unable to predict these experimental results at higher pressures. An apparent preexponential factor was used to fit the experimental data, which was a function of total pressure and the preexponential factor obtained at atmospheric pressure

$$k_{0,p} = k_0\left(\frac{P}{P_0}\right)^q \tag{11}$$

The values of the parameter "*q*" for each oxygen carrier and reaction are showed in Table 3.

Results

Kinetic determination. The kinetic parameters for the reduction of the Cu10Al-I oxygen carrier have been determined in a previous work,[16] and are shown in Table 3. This section focuses in the kinetic determination for the reduction reaction of the other two oxygen carriers (Ni40Al-FG and Fe60Al-FG). To obtain the kinetic parameters, experiments were done at temperatures in the range 973-1223 K, using different mixtures H_2+H_2O or CO+CO_2. To determine the effect of the fuel gas concentration on the reduction reaction rate, several experiments were carried out at 1223 K with different CO or H_2 concentrations. As an example, Figure 4 shows the conversion versus time curves obtained with different temperatures or fuel concentrations. Experimental data are represented by symbols and model

predictions using the kinetic parameters finally obtained are represented as continuous lines. The solid conversion was complete in all of the cases, and the reaction rate increased with increasing the fuel gas concentration or temperature. The effect of the gas product on the reduction reaction was also analyzed. The H_2O or CO_2 concentration was varied while the H_2 or CO concentration was maintained constant. It was concluded that the gas products did not affect the reduction reaction rates of the oxygen carriers.

Considering the reaction controlled by the chemical reaction, the values of the time for complete conversion, τ, were obtained from the slope of the plot of $1-(1-X_r)^{1/3}$ versus t, see equation 5. The kinetics parameters for the reduction of the oxygen carriers with H_2 and CO, showed in Table 3, were obtained from an analysis of τ values[16] obtained for different gas concentrations and temperatures. The activation energies determined for these reactions were low, with values ranging from 14 to 33 kJ/mol. The reaction order depended on the reacting gas, and values from 0.5 to 1 were found.

Comparison of Reactivity and Reaction Rate for use of H_2 or CO. The study carried out about reactivity showed the different behavior obtained with CO or H_2 for the three oxygen carriers. It must be considered that the reactivity of the oxygen carrier is related with the solid inventory needed in the fuel reactor to fully convert the fuel gas to H_2O and/or CO_2. Table 3 shows the values for the reactivity, dX_r/dt, for the different oxygen carriers and gases. For comparison purposes, the values of $dX_r dt$ were calculated for an average gas concentration of 20 vol% and $X_r = 0.3$, which may be normal values for a CLC system.[17] The reaction for the solid proceed faster for the copper-based oxygen carrier than for the nickel- and iron-based oxygen carrier. Moreover, to better compare among oxygen carriers, the reaction rate was defined as a rate of oxygen transfer, i.e. the mass of oxygen transferred per kg of oxygen carrier and second,

$$\left(-r_o\right) = R_{OC}\left[\frac{dX_r}{dt}\right] \tag{12}$$

Thus, the rate of oxygen transfer of the oxygen carriers, $(-r_o)$, is a function of the reactivity, dX_r/dt, and the transport capacity of the oxygen carrier, R_{OC}. Figure 5 shows the rates of oxygen transfer for X_r= 0.3 obtained as a function of the gas concentration for the three oxygen carriers used in this work, at atmospheric pressure and 2.0 MPa. In this Figure, the rate of oxygen transfer is expressed as the kg of oxygen reacted per 100 kg of oxygen carrier and minute, i.e. % min^{-1}. The reactivity at 2.0 MPa was obtained from the results presented in a previous work.[21] It can be observed that the dependence of reactivity with the gas concentration is not linear when the reaction order is different to 1 (see Table 3).

In general, the reactivity with H_2 was higher than with CO for the three oxygen carriers. However, the opposite tendency was observed for Ni40Al-FG at high gas concentration and for Fe60Al-FG at high total pressure. On the other hand, the reactivity followed the sequence Cu10Al-I > Fe60Al-FG > Ni40Al-FG, see dX_r/dt in Table 3. However, the difference in reactivity, dX_r/dt, was not translated to the rate of oxygen transfer, $(-r_o)$. For example, the reactivity, dX_r/dt, for the reduction of Fe60Al-FG with 20% H_2 is about 2.5 times faster than the reaction for Ni40Al-FG , but the rate of oxygen transfer, $(-r_o)$, are in the same order for both oxygen carriers, due to the highest oxygen transport capacity, R_{OC}, of the Ni-based oxygen carrier. In this sense, the reactivity of the Cu10Al-I oxygen carrier was similar to that of the Ni40Al-FG, even the metal oxide content for Cu10Al-I was only 10 wt%. In general, the three oxygen carriers were very reactive and suitable to be used for syngas combustion in a CLC system.

The rate of oxygen transfer at 2 MPa is also shown in Figure 5. A higher pressure produces an increase in the molar concentration of gas, thus an important increase in the reactivity of the oxygen carriers should be expected. However, the rates of oxygen transfer were similar to that obtained at atmospheric pressure, and even lower in some cases, e.g. for the reduction of Fe60Al-FG with H_2 or Ni40Al-FG with CO. Therefore, the reactivity of the oxygen carrier at pressure must be evaluated for each specific case, and should not be extrapolated from results obtained at atmospheric pressure.[21]

For comparison purposes, the rate of oxygen transfer of the three oxygen carriers with methane[17] was also shown in Figure 5. A different behaviour for each oxygen carrier was observed. The rate of oxygen transfer of Fe60Al-FG with methane was lower than with H_2 and CO. Similar results have been obtained in other works.[22,25] On the contrary, the rate of oxygen transfer of Ni40Al-FG with methane was noticeably higher than with H_2 and CO, because the catalytic effect of metallic Ni on intermediate reactions during CH_4 combustion and the higher oxygen stoichiometry for CH_4 than for CO and H_2.[32] Finally, the Cu10Al-FG exhibited a similar rate of oxygen transfer with methane and H_2.

Reduction reaction with CO and H_2 mixtures. The experiments showed above for kinetic determination were accomplished using a single reacting gas, CO or H_2. However, in a CLC system that use synthesis gas the oxygen carrier is in contact with several gases simultaneously, i.e. CO, H_2, and products CO_2 and H_2O. The same situation could occur during solid fuels or natural gas combustion where CO and H_2 can appear by lateral reactions. This fact could be of high importance when using Ni-based oxygen carriers. To determine the reactivity of the oxygen carriers with mixtures of CO and H_2, several experiments were carried out both in TGA and PTGA using different mixtures of CO, H_2, CO_2, and H_2O.

Table 2 shows the concentrations of H_2 and CO used in the reacting gas. In the experiments at atmospheric pressure, the concentrations of CO and H_2 in the gas mixture were chosen based on the relative reactivity of the individual gases. The three selected conditions corresponded with the following situations: (c1) the reaction rate for H_2 was higher than for CO; (c2) both reaction rates were approximately equal; and (c3) the reaction rate for H_2 was lower than for CO. Figure 6 shows the conversion vs time curves obtained with the three oxygen carriers. To analyze the reactivity of the oxygen carriers in gas mixtures of H_2 and CO, Figure 6 shows the conversion vs time predicted assuming the sum of the reaction rates with CO and H_2, as well as the curves corresponding to each one of the gases separately, H_2 or CO, using the individual gas concentration existing in the gas mixture.

The theoretical curves assuming the addition of the reaction rates for H_2 and CO were obtained from equations 5 and 6, but using a value for τ obtained as

$$\tau = \left(\frac{1}{\tau_{H_2}} + \frac{1}{\tau_{CO}} \right)^{-1} \quad (13)$$

The theoretical curves obtained assuming the sum of reaction rates predicted adequately the experimental curves for the Cu10Al-I and Fe60Al-FG oxygen carriers. However, the curves predicted for Ni45Al-FG were always higher than the experimentally obtained. In this case, the experimental curves corresponded to the obtained with the gas that faster reacted within the gas mixture.

The use of syngas in a pressurized CLC system for power generation would have several advantages with respect to the atmospheric operation, as previously has been mentioned. Usually, the IGCC process is carried out at pressures in the range 2-3 MPa, and the reactivity must be determined at the operating pressure of the industrial plant.[21] In the present work, the reactivity of the oxygen carriers was finally determined in a PTGA system with a mixture of H_2 and CO. The experiments were carried out at 1073 K and 2 MPa, and the gas composition (c4) shown in Table 2. Figure 7 shows the conversion-time curves obtained experimentally with the three oxygen carriers. In addition, the theoretical curves corresponding to each one of the gases separately at the same gas concentration to the used in the gas mixture, i.e. 10 vol% H_2 or 10 vol% CO, were showed, as well as the predicted curves assuming that the reactivity of the oxygen carrier in the gas mixture is the sum of reactivities of each gas separately, H_2 and CO. At these conditions, $\left(-r_{o,H_2}\right) > \left(-r_{o,CO}\right)$ for Cu10Al-I and Ni40Al-FG oxygen carriers, and approximately equal for Fe60Al-FG. For the Cu- and Fe-based oxygen carriers, it was observed that the experimental curves obtained with the mixture H_2+CO agreed with the theoretical curve predicted using the sum of reactivities of each reacting gas separately. On the contrary, for the Ni-based oxygen carrier the X_r-t curve was similar to the obtained with H_2, which reacted faster than the CO at the existing experimental conditions. These results agree with those observed at atmospheric pressure.

The behaviour observed during the reduction of the Ni-based oxygen carrier with H_2 and CO mixtures is difficult to explain at this point, and more work should be done to know the amounts of H_2 and CO reacted at these conditions. It is important to know this fact for reactor design purposes. However, when the WGS equilibrium is fulfilled in the entire reactor, which could be the case for Ni-based oxygen carriers, it is not important to know exactly the amounts of H_2 and CO reacted at each position inside the reactor, because the gas composition is determined by the oxygen transferred and the WGS equilibrium. Uniquely the knowledge of the reactivity of the oxygen carrier in the H_2 and CO mixture it is necessary; and this is the reactivity of the gas reacting faster. Therefore, in the subsequent analysis, it was assumed that the gas, H_2 or CO, with a lower reactivity did not react with the oxygen carrier, and only the gas with higher reaction rate reacted.

Applications for design. The reactivity data obtained can be used to design the fuel reactor in a CLC system, i.e. to obtain the solids inventory necessary to fully convert the gas fuel. For a preliminary calculation, the two phase theory for a fluidized bed[31] was considered with the following assumptions: (1) perfect mixing of the solids; (2) gas plug flow; and (3) no resistance to the gas exchange between bubble and emulsion phases in the fluidized bed. The solid inventory for one reacting gas can be calculated from[16,17]

$$m_{OC}^{*} = y_g \Delta X_g \frac{2dM_O}{R_{OC}\Delta H_c^0}\frac{\bar{\tau}}{\Phi} = y_g \Delta X_g \frac{2dM_O}{\Delta H_c^0}\frac{\delta}{\Phi\left(-\bar{r}_0\right)} \qquad (14)$$

where the average rate of oxygen transfer, $\left(-\bar{r}_0\right)$, is calculated at X_r=0 and using a mean concentration in the reactor (see $\bar{C}$ in Table 4). The mean concentration, $\bar{C}$, depends on the reaction order of the reacting gas, and the reaction rate at this gas concentration gives an idea about the average reactivity of the oxygen carrier in the reactor, see Figure 5. The parameter δ comes from derivation of equations 5 and 6 (see equations 8 and 9), and takes the value 1 when the SCM for plate-like geometry is used, or 3 for spherical geometry. The parameter Φ in equation 14 is defined as the characteristic

reactivity, which depends on the solid conversion at the inlet, $X_{r,in}$, and the conversion variation in the reactor, ΔX_r.[17] This parameter takes into account for the residence time and the average conversion of the particles in the reactor, and it was calculated assuming perfect mixing of solids. For comparison purposes, the solids inventories were calculated for a value of $\Delta X_r = 0.3$, which may be normal values for a CLC system,[17] and assuming the complete oxidation of the oxygen carrier in the air reactor, i.e. $X_{r,in}=0$. At these conditions, the values for Φ were 0.96 for the SCM with plate-like geometry (Cu10Al-I) and 2.3 for the SCM with spherical geometry (Fe60Al-FG and Ni40Al-FG).

Table 3 shows the solids inventories for H_2 and CO at 0.1 and 2.0 MPa to obtain a gas conversion of $X_g = 0.995$ for Cu10Al-I and Fe60Al-FG, or $X_g = 0.98$ for Ni40Al-FG. The lower X_g used for Ni40Al-FG was because thermodynamic limitations to fully convert the H_2 and CO to H_2O and CO_2 using Ni-based oxygen carriers. At 1223 K, the maximum conversion of the fuel gases with Ni-based oxygen carriers is 0.993 for H_2 and 0.989 for CO. In general, the solids inventories for H_2 are lower than those for CO, because the higher reactivity of H_2. In any case, the reactivity was high enough to obtain very low solids inventories, ranging from 17 to 41 kg/MW at atmospheric pressure, and from 14 to 43 at 2.0 MPa.

In syngas combustion, the fuel gas is composed by a mixture of CO, H_2, CO_2 and H_2O. In this case, a mass balance of the solid and gas in the fuel and air reactors has been done to obtain the solid inventory. According to the assumptions above showed, the differential mass balance on the oxygen atoms between the height *z* and *z*+dz yields:

$$u_g \frac{\partial C_{H_2}}{\partial z} + \frac{1}{2d}(1-\varepsilon_b)\rho_{m,O}\left[\frac{\Phi}{\delta}\frac{\partial X_r}{\partial t}\bigg|_{X_r=0}\right]_{H_2,z} = 0 \qquad (15a)$$

$$u_g \frac{\partial C_{CO}}{\partial z} + \frac{1}{2d}(1-\varepsilon_b)\rho_{m,O}\left[\frac{\Phi}{\delta}\frac{\partial X_r}{\partial t}\bigg|_{X_r=0}\right]_{CO,z} = 0 \qquad (15b)$$

The height, *z*, at which there is a determined concentration, is a function of the fluidized bed porosity, ε_b. However, considering the assumptions showed above, the gas concentration is determined by the mass of oxygen carrier existing below to height *z*. To avoid the dependency with the bed porosity, equations 15a and 15b have be rewritten as a function of the mass of oxygen carrier, m_{OC}^*. Taking as reference 1 MW of fuel gas, the differential mass balance is transformed into

$$\frac{10^3}{\Delta H_c^0}\frac{\partial y_{H_2}}{\partial m_{OC}^*}+\frac{1}{2\cdot 10^{-3} dM_O}\frac{\Phi}{\delta}\left(-r_{0,H_2}\right)_{m_{OC}^*}=0 \quad (16a)$$

$$\frac{10^3}{\Delta H_c^0}\frac{\partial y_{CO}}{\partial m_{OC}^*}+\frac{1}{2\cdot 10^{-3} dM_O}\frac{\Phi}{\delta}\left(-r_{0,CO}\right)_{m_O^*}=0 \quad (16b)$$

The initial conditions for equations 16a and 16b are $y_{H_2}=y_{0,H_2}$ and $y_{CO}=y_{0,CO}$ at $m_{OC}^*=0$, corresponding to *z* = 0. From the analysis above described about the reactivity of oxygen carriers with H_2 and CO mixtures, two different behaviours have been identified. The reaction pattern of H_2 and CO in a mixture of gases will have important consequences on the amount of H_2 and CO reacted in the fuel reactor, and should be considered in the reactor design. Thus, for the Cu10Al-I and Fe60Al-FG oxygen carriers, the reaction rate can be considered as a sum of the individual reaction rates corresponding to the concentrations of H_2 and CO. For the Ni40Al-FG oxygen carrier, the reactivity corresponds to the gas which the oxygen carrier reacts faster at the conditions of the reacting gas mixture, H_2 or CO, and the gas i with a lower reaction rate does not react with the oxygen carrier, and $\left(-r_{0,i}\right)_{m_O^*}$ = 0. As the reaction rate varies with the gas concentration, the reacting gas, H_2 or CO, will depend on the actual gas concentration.

The syngas composition (CO, H_2, CO_2 and H_2O) depends on the gasifier type. To simulate the combustion behaviour of syngas in a CLC process, a pattern gas for an entrained bed gasifier has been chosen, consisting in 45 vol% CO, 30 vol% H_2, 10 vol% CO_2 and 15 vol% H_2O with a combustion enthalpy of 200 kJ mol^{-1}. The operating conditions in the fuel reactor were 1223 K and 2.0 MPa.

Firstly, the WGS equilibrium, reaction 1, was not considered. Figure 8 (a) shows the profiles of H_2 and CO concentration and the fuel gas conversion as a function of the mass of oxygen carrier inside the reactor, m_{OC}^*, for the three oxygen carriers considered in this work. The conversion of the fuel gas was obtained as,

$$X_g = \frac{\left(y_{0,H_2} - y_{H_2}\right) + \left(y_{0,CO} - y_{CO}\right)}{y_{0,H_2} + y_{0,CO}} \tag{17}$$

The oxygen carriers exhibited different reaction behaviour, see Figure 8 (a). For Cu10Al-I and Fe60Al-FG, the total reaction rate was the sum of the individual reaction rates, $\left(-r_{o,syngas}\right) = \left(-r_{o,H_2}\right) + \left(-r_{o,CO}\right)$, and H_2 and CO react from the beginning. For Cu10Al-I, the initial reaction rate with H_2 is higher than for CO, and H_2 disappear faster. For m_{OC}^* >10 kg MW^{-1}, the only reacting gas is CO. The solids inventory to obtain a high conversion of gas, e.g. 99.5%, is limited by the reactivity of the oxygen carrier with CO, as it is shown in Figure 8 (a). For Fe60Al-FG, the initial reactivity with CO is higher than for H_2. However, as the reaction order for the CO reaction (n=1) is higher than that for the H_2 reaction (n=0.8), the reaction rate for CO becomes lower at high gas conversion. On the other hand, for Ni40Al-FG it was considered that the gas, H_2 or CO, with a lower reactivity did not react with the oxygen carrier. In this case, in the range values of m_{OC}^* from 0 to 4 kg MW^{-1} the reactivity with CO is lower than that for H_2, and the CO concentrations remains constant whereas the H_2 concentration decreases. At $m_{OC}^* \approx 4$ kg MW^{-1} the reaction rate for H_2 becomes equal to that for CO, and both gases react with the same reactivity, corresponding to any of them, until the maximum conversion of syngas, which is limited by thermodynamic to X_g = 0.988.

Figure 8 shows the solid inventory to obtain a certain fuel gas conversion. Table 4 shows the solids inventory needed when using H_2, CO or syngas for a fuel gas conversion value of 99.5% for Cu10Al-I and Fe60Al-FG, and 98% for Ni40Al-FG . In general, the solids inventory for syngas is higher than

those obtained for the individual gases, H_2 or CO. This difference is noticeable for Ni40Al-FG, where a solids inventory of 49 kg MW^{-1} was obtained for syngas, because the reaction rate is lower than that corresponding to the addition of reaction rates for H_2 and CO. In this case, if the reaction rate was the sum of those for H_2 and CO, the solids inventory would be 36 kg MW^{-1}. The lower solids inventory was obtained for Fe60Al-FG, because the average reaction rate for the gas mixture was the highest of the three oxygen carriers.

However, in a gas mixture composed by CO, H_2, CO_2 and H_2O, the WGS equilibrium given by reaction 1 should be considered. This reaction changes the gas profiles concentration, and therefore the reaction rate of the oxygen carrier inside the reactor. As consequence, solids inventory are different depending if WGS equilibrium is or not considered. The effect of WGS reaction on the behaviour of the reactor depends on the relative reaction rate between the reaction of H_2 and CO with the oxygen carrier and the rate of WGS reaction. In the above showed results, it was assumed that the rate of WGS reaction was much lower than the reaction of gases with the solid, and the change in gas concentration by WGS reaction was negligible. To analyze the effect of WGS equilibrium, later it was assumed that WGS reaction is in instantaneous equilibrium. Figure 8 (b) shows the concentration profiles obtained in the reactor considering WGS reaction at equilibrium. In comparison with Figure 8 (a), it can be observed than the gas mixture is enriched in the gas with higher reaction rate, e.g. H_2 for Cu10Al-I or CO for Fe60Al-FG, because the gas disappeared by the reaction with the solid is partially compensated by the generated by WGS reaction. The consequence of this fact is an increase in the average reaction rate of the oxygen carrier in the reactor, and therefore a decrease in the solids inventory with respect to the omission of WGS equilibrium. The solids inventories considering the WGS equilibrium were in the range 19-34 kg MW^{-1}, as showed in Table 4.

For the three oxygen carriers considered in this work, the solids inventory needed to fully convert the syngas to CO_2 and H_2O are relatively low, and are potential candidates to be used in a CLC system

burning syngas both at atmospheric and pressurized conditions. However, it must be remarked that these values correspond to conditions where the resistance to the gas exchange between the bubble and emulsion phases has been considered negligible. In real systems, if the resistance to the gas exchange between the bubble and emulsion phases is important higher solids inventories would be necessary.

Conclusions

The reactivity of the reduction reaction for three promising oxygen carriers (Cu10Al-I, Ni40Al-FG and Fe60Al-FG) was determined by thermogravimetric analysis using H_2, CO, and H_2+CO mixtures. The oxygen carriers exhibited very high reactivity during the reduction reaction. Although the reactivity was higher for Cu10Al-I than for Ni40Al-FG and Fe60Al-FG, the rate of oxygen transport was similar for the three oxygen carriers, because of the differences on the oxygen transport capacity. Average values for the transference rates of oxygen were about 20-25 % min^{-1} for H_2 and 10-15 % min^{-1} for CO. The shrinking-core model for spherical or plate grain geometry of reacting particle with chemical reaction control was used to determine the kinetics parameters. The reaction order for the reduction reaction was in the range 0.5-1, and low activation energies, from 14 to 33 kJ mol^{-1}, were found.

Two different behaviours were observed during the reduction reaction with syngas, i.e. CO+H_2. For Cu10Al-I and Fe60Al-FG, the reaction rate of the oxygen carrier was the addition of the individual rates for H_2 and CO. However, for Ni40Al-FG, the reaction rate corresponded to that of the gas reacting faster, H_2 or CO, depending on the actual gas concentration. These results were observed both at atmospheric and pressurized conditions. A preliminary estimation of the solids inventory for the use of syngas in the fuel reactor of a CLC system gave values in the range of 19-34 kg MW^{-1} when the WGS equilibrium was considered be instantaneous.

Acknowledgements

This research was conducted with financial support from the Diputación General de Aragón (Project No. PIP023/2005), CICYT (Project No. CTQ2004-04034), and from the GRACE (Grangemouth Advanced CO2 Capture) Project coordinated by BP and funded by the EU (ENK5-CT-2001-00571) and by the CCP (CO2 Capture Project), a partnership of BP, ChevronTexaco, EnCana, Eni, Norsk Hydro, Shell, Suncor, and Statoil.

References

(1) *IPCC Special Report on Carbon Dioxide Capture and Storage*; Cambridge University Press: New York, NY, 2005. Available on the web: http://www.ipcc.ch

(2) Eide, L.I.; Anheden, M.; Lyngfelt, A.; Abanades, C.; Younes, M.; Clodic, D.; Bil,l A.A.; Feron, P.H.M.; Rojey, A.; Giroudière, F. *Oil & Gas Science and Technology* **2005**, 60, 497-508.

(3) *The CO_2 Capture and Storage Project (CCP) for Carbon Dioxide Storage in Deep Geologic Formations For Climate Change Mitigation, Volume I – Capture and Separation of Carbon Dioxide From Combustion Sources*; Thomas, D., Benson, S., Eds,; Elsevier: New York, 2005; Vol 1.

(4) Kerr, HR. Capture and separation technologies gaps and priority research needs. In *Carbon Dioxide Capture for Storage in Deep Geologic Formations - Results from the CO_2 Capture Project;* Thomas, D., Benson, S., Eds,; Elsevier: New York, 2005; Vol 1, Chapter 38, pp 655-660.

(5) Copeland, R. J.; Alptekin, G.; Cessario, M.; Gerhanovich, Y. A Novel CO_2 Separation System. *Proceedings of the First National Conference on Carbon Sequestration*, Washignton, DC, 2001; available in the web: http://www.netl.doe.gov/publications/proceedings/01/carbon_seq/carbon_seq01.html

(6) Jin, H.; Ishida, M. *Fuel* **2004**, 83, 2411-2417.

(7) Wolf, J.; Anheden, M.; Yan, J. Performance Analysis of Combined Cycles with Chemical Looping Combustion for CO2 Capture. In *International Pittsburg Coal Conference*, Newcastle, New South Wales, Australia, 2001.

(8) Lyngfelt, A.; Leckner, B.; Mattison, T. *Chem. Eng. Sci.* **2001**, 56, 3101-3113.

(9) Ishida, M.; Jin, H. *J. Chem. Eng. Japan* **1994**, 27, 296-301.

(10) Ishida, M.; Jin, H.; Okamoto, T. *Energy Fuels* **1996**, 10, 958-963.

(11) Ishida, M.; Jin, H. *Ind. Eng. Chem. Res.* **1996**, 35, 2469-2472.

(12) Ishida, M; Jin, H.; Okamoto, T. *Energy Fuels* **1998**, 12, 223-229.

(13) Jin, H.; Okamoto, T.; Ishida, M. *Energy Fuels* **1998**, 12, 1272-1277.

(14) Villa R, Cristiani C, Groppi G, Lietti L, Forzatti P, Cornaro U, Rossini S. *J Molecular Cat A: Chem* **2003**, 204-5, 637-646.

(15) de Diego, L.F.; García-Labiano, F.; Adánez, J.; Gayán, P.; Abad, A.; Corbella, B.M.; Palacios, J.M. *Fuel* **2004**, 83, 1749-1757.

(16) García-Labiano, F.; de Diego, L.F.; Adanes, J.; Abad, A.; Gayán, P. *Ind. Eng. Chem. Res.* **2004**, 43, 8168-8177.

(17) Abad A.; Adánez, J.; García-Labiano, F.; de Diego, L.F.; Gayán, P.; Celaya, J. *Chem Eng Sci*. **2007**, 62, 533-549.

(18) Readman, J.E.; Olafsen, A.; Smith, J.B.; Blom, R. *Energy Fuels* **2006**, 20, 1382-1387.

(19) Jin, H.; Okamoto, T.; Ishida, M. *Ind. Eng. Chem. Res.* **1999**, 38, 126-132.

(20) Jin, H.; Ishida M. *Int J Hyd Energy* **2001**, 26, 889-894.

(21) García-Labiano, F.; Adánez, J.; de Diego, L.F.; Gayán, P.; Abad, A. *Energy Fuels* **2006**, 20, 26-33.

(22) Mattisson, T.; Johansson, M.; Lyngfelt, A. CO_2 Capture from Coal Combustion Using Chemical-Looping Combustion – Reactivity Investiation of Fe, Ni and Mn Based Oxygen Carriers Using Syngas.

Proceedings of the *31st International Technical Conference on Coal Utilization & Fuel Systems*; Clearwater, Florida, USA, 2006.

(23) Abad, A.; Mattisson, T.; Lyngfelt, A.; Rydén, M. *Fuel* **2006**, 85, 1174-1185.

(24) Johansson, E.; Mattisson, T.; Lyngfelt, A.; Thunman, H. *Chem. Eng. Res. Des.* **2006**, 84, 819-827.

(25) Abad, A.; Mattisson, T.; Lyngfelt, A.; Johansson, M. *Fuel* **2007**, 86, 1021-1035.

(26) Leion, H.; Mattisson, T.; Lyngfelt, A. Fuel **2007,** *available online 28 December 2006*.

(27) Cho P, Mattisson T, Lyngfelt A. *Fuel* **2004**, 83, 1215-1225.

(28) Jerndal, E.; Mattisson, T.; Lyngfelt, A. *Chem. Eng. Res. Des.* **2006**, 84, 795-806.

(29) Patrick, V.; Gavalas, G.R.; Sharma, P.K. *Ind. Eng. Chem. Res.* **1993**, 32, 519-532.

(30) García-Labiano, F.; de Diego, L.F.; Adánez, J.; Abad, A.; Gayán, P. *Chem. Eng. Sci.* **2004**, 60, 851-862.

(31) Levenspiel, O. *Chemical Reaction Engineering*; John Wiley and Sons, Inc., New York, 1981.

(32) Mattisson, T.; Johansson, M,; Lyngfelt, A. *Fuel* **2006**, 85, 736-747.

Nomenclature

b = stoichiometric factor in the reduction reaction of metal oxide (mol of MeO per mol of fuel gas)

C = gas concentration (mol m^{-3})

C_{eq} = gas concentration at equilibrium conditions (mol m^{-3})

$\overline{C}$ = average gas concentration (mol m^{-3})

d = stoichiometric factor for the combustion of fuel gas with oxygen (mol of O_2 per mol of fuel gas)

E = activation energy (J mol^{-1})

k = chemical reaction rate constant (mol^{1-n} m^{3n-2} s^{-1})

k_0 = preexponential factor of the chemical reaction rate constant (mol^{1-n} m^{3n-2} s^{-1})

$k_{0,p}$ = preexponential factor of the chemical reaction rate constant at pressurized conditions (mol^{1-n} m^{3n-2} s^{-1})

L = layer thickness of the reacting solid (m)

m = mass of sample (kg)

m_{ox} = mass of the fully oxidized oxygen carrier (kg)

m_{red} = mass of the fully reduced oxygen carrier (kg)

m^*_{OC} = mass of oxygen carrier per MW of fuel (kg MW^{-1})

M_O = atomic weight of the oxygen (g mol^{-1})

n = reaction order

P = total pressure (Pa)

P_0 = reference pressure (P_0 = 101325 Pa)

q = exponent in equation 11

r_g = grain radius (m)

$(-r_o)$ = rate of oxygen transfer (kg O kg OC^{-1} s^{-1})

$(-\bar{r}_0)$ = average rate of oxygen transfer at $X_r = 0$ and $\bar{C}$ (kg O kg OC^{-1} s^{-1})

R_g = ideal gas constant (= 8.314 J mol^{-1} K^{-1})

R_o = oxygen transport capacity of the active metal oxide (kg O kg MeO^{-1})

R_{OC} = oxygen transport capacity of the oxygen carrier (kg O kg OC^{-1})

S_{BET} = specific surface area of reacting solid (m^2 g^{-1})

t = time (s)

T = temperature (K)

u_g = gas velocity (m s^{-1})

X_g = gas conversion

X_r = solid conversion

$\bar{X}_{r,in}$ = average solid conversion at the inlet of the fuel reactor

y_i = molar fraction of gas i

z = axial position in the reactor (m)

Greek letters

δ = constant parameter coming from derivation of equations 5 and 6 , see equations 8 and 9

ΔH_c^0 = standard heat of combustion of the gas fuel (kJ mol^{-1})

ΔX_g = variation of gas conversion

ΔX_r = variation of solid conversion

ε_b = bed porosity

Φ = characteristic reaction rate, as defined in reference (17)

ρ_s = real density of solid (g m^{-3})

ρ_m = molar density of metal oxide in the solid (mol of MeO per m^3 of solid)

$\rho_{m,O}$ = molar density of oxygen in the oxygen carrier (at-gr of oxygen per m^3 of particle)

τ = time for complete solid conversion (s)

$\bar{\tau}$ = time for complete solid conversion for the reaction at $\bar{C}$ (s)

ω = fractional mass of the oxygen carrier with respect to the mass of fully oxidized oxygen carrier

Tables

Table 1. Properties of the oxygen carriers.

	Cu10Al-I	Fe60Al-FG	Ni40Al-FG
Active MeO content (wt %)	10	60	40
Particle size (mm)	0.17	0.15	0.2
Porosity	0.57	0.30	0.36
Specific surface area BET ($m^2\ g^{-1}$)	41.3	2.5	0.8
Solid density (kg m^{-3})	4180	4650	5380
Oxygen transport capacity, R_{OC}	0.02	0.04	0.084

Table 2. Experimental conditions in TGA and PTGA tests when CO and H_2 were simultaneously present in the reacting gases.

	P_T = 0.1 MPa						P_T = 2 MPa
	T = 1073 K			T = 1223 K			T = 1073 K
	c1	c2	c3	c1	c2	c3	c4
H_2	20	5	5	20	5	5	10
CO	5	15	30	5	15	30	10
CO_2	5	30	55	5	20	40	5
H_2O	20	10	10	30	15	10	5

The balance was N_2

Table 3. Kinetic parameters and reactivity for reduction of Cu10Al-I, Ni40Al-FG and Fe60Al-FG with H_2 and CO.

	Cu10Al-I		Fe60Al-FG		Ni40Al-FG	
	H_2	CO	H_2	CO	H_2	CO
Physical parameters						
ρ_m (mol/m^3)	80402	80402	13089	13089	89290	89290
r_g or L (m)	$4.0\ 10^{-10}$	$4.0\ 10^{-10}$	$2.6\ 10^{-7}$	$2.6\ 10^{-7}$	$6.9\ 10^{-7}$	$6.9\ 10^{-7}$
b	1	1	1	1	1	1
Kinetic parameters						
k_0 (mol^{1-n} m^{3n-2} s^{-1})	$1.0\ 10^{-4}$	$5.9\ 10^{-6}$	$9.0\ 10^{-4}$	$2.5\ 10^{-4}$	$9.3\ 10^{-3}$	$5.2\ 10^{-3}$
E (kJ/mol)	33	14	24	20	26	25
n	0.6	0.8	0.8	1.0	0.5	0.8
Effect of pressure						
q [eq. (11)]	-0.53	-0.83	-1.03	-0.89	-0.47	-0.93
Reactivity[a] (s^{-1})						
dX_r/dt at 0.1 MPa	0.18	0.077	0.10	0.047	0.040	0.028
dX_r/dt at 2.0 MPa	0.22	0.070	0.050	0.065	0.044	0.019

[a] Obtained at 1223 K, 20% reacting gas and X_r = 0.3

Table 4. Average concentration, $\overline{C}$, and solids inventory for the three oxygen carriers with H_2, CO, and a pattern syngas (45 vol% CO, 30 vol% H_2, 10 vol% CO_2, 15 vol% H_2O). T = 1223K; X_g = 0.995 for Cu10Al-I and Fe60Al-FG, or X_g = 0.98 for Ni40Al-FG; ΔX_r = 0.3; and $X_{r,in}$=0.

	Cu10Al-I	Fe60Al-FG	Ni40Al-FG
Average concentration, $\overline{C}$ (%)			
H_2	24.2	19.2	26.6
CO	19.2	14.5	19.2
Solids inventory (kg/MW) at 0.1 MPa			
H_2	16	15	16
CO	34	32	22
Solids inventory (kg/MW) at 2.0 MPa			
H_2	13	30	15
CO	38	23	32
Syngas[a]	43	31	49
Syngas[b]	19	30	34

[a] When WGS equilibrium is not considered

[b] When WGS equilibrium is considered

Captions of the Figures

Figure 1. Chemical-looping combustion.

Figure 2. Iron compound at the equilibrium as a function of the gas composition at 1223 K. Dots represent the experimental conditions in TGA: reduction to FeO ●; reduction to Fe ▲

Figure 3. Effect of the reacting gas on the final product reached upon Fe_2O_3 reduction with Fe60Al-FG. T = 1223 K; $H_2O/H_2 \approx 10$ [5% H_2 + 48% H_2O] (———), $H_2O/H_2 = 0.75$ [40% H_2 + 30% H_2O] (– – – –), $H_2O/H_2 = 0.25$ [40% H_2 + 10% H_2O] (—·—·—·), corresponding to Zone A, B and C in Figure 2, respectively.

Figure 4. Effect of fuel gas concentration and temperature on the conversion vs time curves. (a) Oxygen carrier: Ni40Al-FG; T = 1223 K; CO_2 = 20 vol%; CO concentration = 5 vol% (■), 10 vol% (◆), 40 vol% (▲), 70 vol% (●). (b) Oxygen carrier: Fe60Al-FG; CO = 40 vol%; CO_2 = 20 vol%; Temperature = 973 K (◇), 1073 K (△), 1123 K (○), 1173 K (□), 1123 K (▽). Model predictions (——)

Figure 5. Reaction rates for the reduction reactions as a function of the gas concentration. X_r= 0.3; T=1223 K; Pressure = 0.1 MPa (———), 2.0 MPa (– – – –). Average reactivity in the fuel reactor: H_2 (□), CO (○), CH_4 (◆).

Figure 6. Conversion vs. time curves for H_2 and CO mixtures. T = 1223 K, P = 0.1 MPa. Experimental data (○); predictions using: reaction for H_2 (—·—·—·), reaction for CO (– – – –), reaction for H_2 + CO considering the sum of the individual reaction rates (———).

Figure 7. Conversion versus time curves for H_2 and CO mixture. T= 1073 K, P= 2 MPa, gas concentration: 10 vol% H_2 and 10 vol% CO. Experimental data (○); Model predictions: reaction for H_2

(—·—·–), reaction for CO (− − − −), reaction for H_2 + CO considering the sum of the individual reaction rates (———).

Figure 8. Profiles of H_2 and CO concentration and fuel gas conversion as a function of the mass of oxygen carrier inside the reactor, m_{OC}^{*}. (a) non-considering the WGS equilibrium; (b) considering the WGS equilibrium. Syngas: 45 vol% CO, 30 vol% H_2, 10 vol% CO_2 and 15 vol% H_2O. 1223 K and 2.0 MPa. Gas concentration: H_2 (—·—·–) and CO (− − − −); Fuel gas conversion (———); solid inventory at X_g = 0.995 for Cu10Al-I and Fe60Al-FG or X_g = 0.98 for Ni40Al-FG (·····)

Reduction Kinetics of Cu-, Ni-, and Fe-based Oxygen Carriers Using Syngas ($CO+H_2$) for Chemical-Looping Combustion. Alberto Abad, Francisco García-Labiano, Luis F. de Diego, Pilar Gayán, Juan Adánez

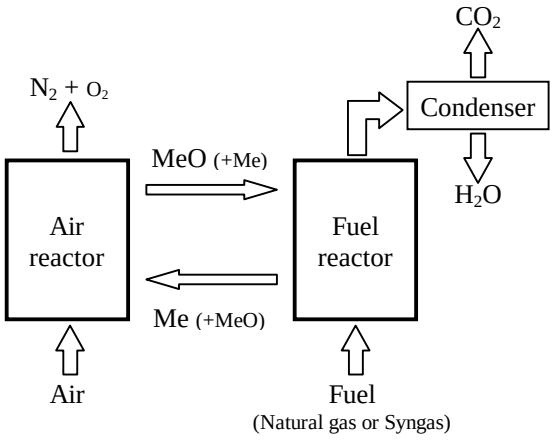

Figure 1. Chemical-looping combustion.

Reduction Kinetics of Cu-, Ni-, and Fe-based Oxygen Carriers Using Syngas ($CO+H_2$) for Chemical-Looping Combustion. Alberto Abad, Francisco García-Labiano, Luis F. de Diego, Pilar Gayán, Juan Adánez

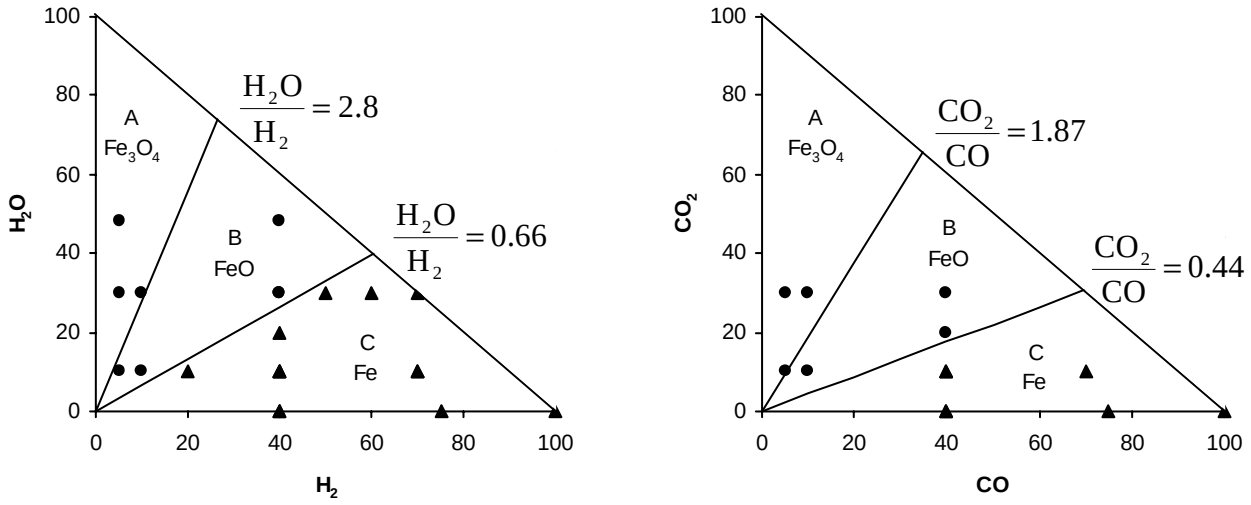

Figure 2. Iron compound at the equilibrium as a function of the gas composition at 1223 K. Dots represent the experimental conditions in TGA: reduction to FeO ●; reduction to Fe ▲

Reduction Kinetics of Cu-, Ni-, and Fe-based Oxygen Carriers Using Syngas ($CO+H_2$) for Chemical-Looping Combustion. Alberto Abad, Francisco García-Labiano, Luis F. de Diego, Pilar Gayán, Juan Adánez

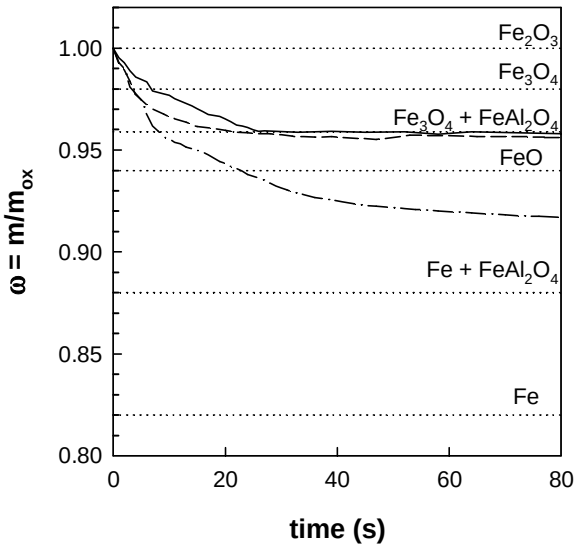

Figure 3. Effect of the reacting gas on the final product reached upon Fe_2O_3 reduction with Fe60Al-FG. T = 1223 K; $H_2O/H_2 \approx 10$ [5% H_2 + 48% H_2O] (———), $H_2O/H_2 = 0.75$ [40% H_2 + 30% H_2O] (– – – –), $H_2O/H_2 = 0.25$ [40% H_2 + 10% H_2O] (—·—·—·), corresponding to Zone A, B and C in Figure 2, respectively.

Reduction Kinetics of Cu-, Ni-, and Fe-based Oxygen Carriers Using Syngas ($CO+H_2$) for Chemical-Looping Combustion. Alberto Abad, Francisco García-Labiano, Luis F. de Diego, Pilar Gayán, Juan Adánez

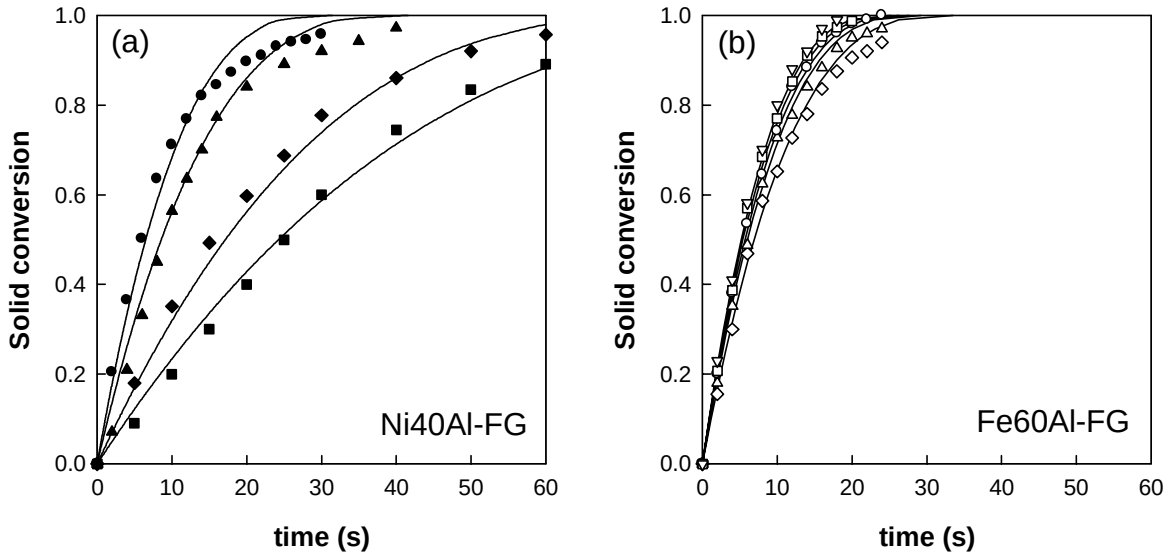

Figure 4. Effect of fuel gas concentration and temperature on the conversion vs time curves. (a) Oxygen carrier: Ni40Al-FG; T = 1223 K; CO_2 = 20 vol%; CO concentration = 5 vol% (■), 10 vol% (◆), 40 vol% (▲), 70 vol% (●); N_2 to balance. (b) Oxygen carrier: Fe60Al-FG; CO = 40 vol%; CO_2 = 20 vol%; Temperature = 973 K (◇), 1073 K (△), 1123 K (○), 1173 K (□), 1223 K (▽). Model predictions (——)

Reduction Kinetics of Cu-, Ni-, and Fe-based Oxygen Carriers Using Syngas ($CO+H_2$) for Chemical-Looping Combustion. Alberto Abad, Francisco García-Labiano, Luis F. de Diego, Pilar Gayán, Juan Adánez

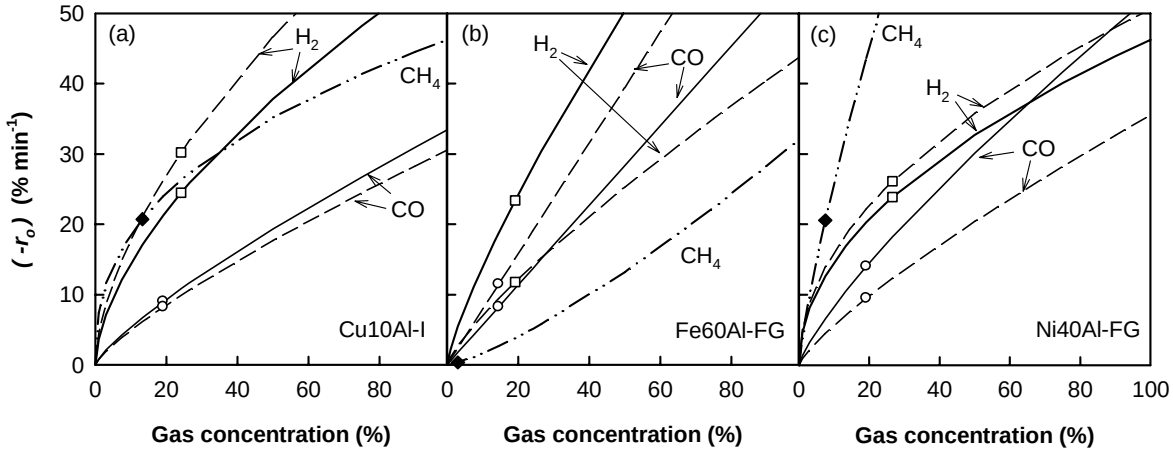

Figure 5. Reaction rates for the reduction reactions as a function of the gas concentration. X_r= 0.3; T=1223 K; Pressure = 0.1 MPa (———), 2.0 MPa (– – – –). Average reactivity in the fuel reactor: H_2 (▫), CO (°), CH_4 (◆).

Reduction Kinetics of Cu-, Ni-, and Fe-based Oxygen Carriers Using Syngas ($CO+H_2$) for Chemical-Looping Combustion. Alberto Abad, Francisco García-Labiano, Luis F. de Diego, Pilar Gayán, Juan Adánez

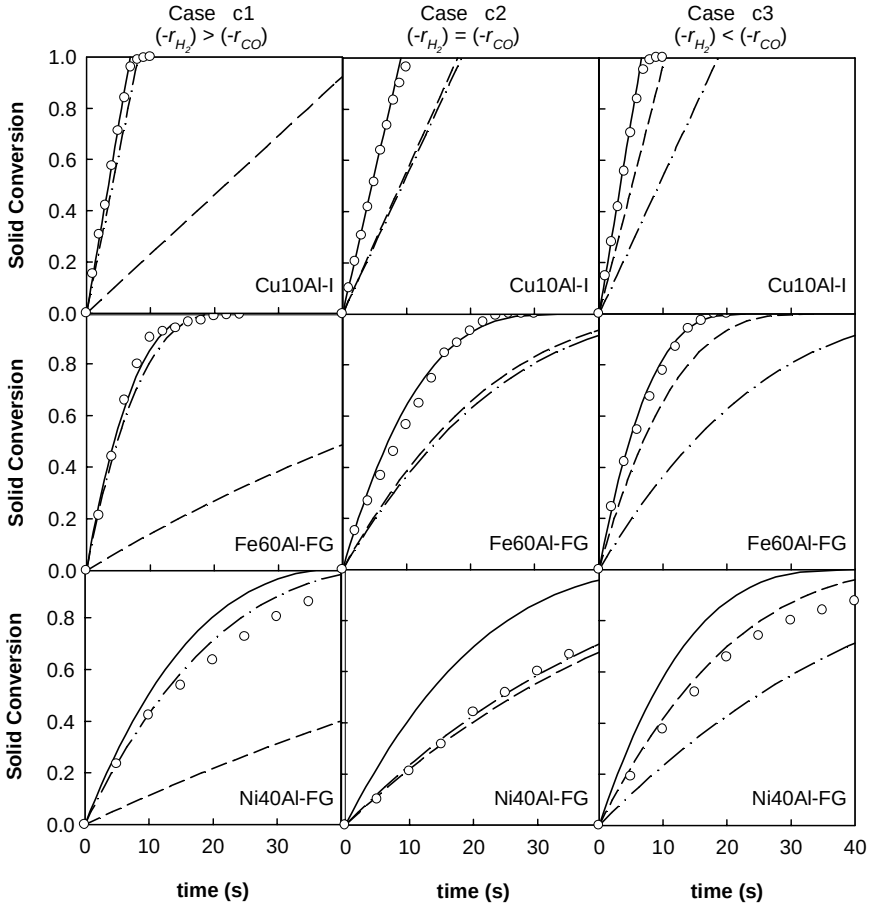

Figure 6. Conversion vs. time curves for H_2 and CO mixtures. T = 1223 K, P = 0.1 MPa. Experimental data (◦); predictions using: reaction for H_2 (—·—·—·), reaction for CO (− − − −), reaction for H_2 + CO considering the sum of the individual reaction rates (———).

Reduction Kinetics of Cu-, Ni-, and Fe-based Oxygen Carriers Using Syngas ($CO+H_2$) for Chemical-Looping Combustion. Alberto Abad, Francisco García-Labiano, Luis F. de Diego, Pilar Gayán, Juan Adánez

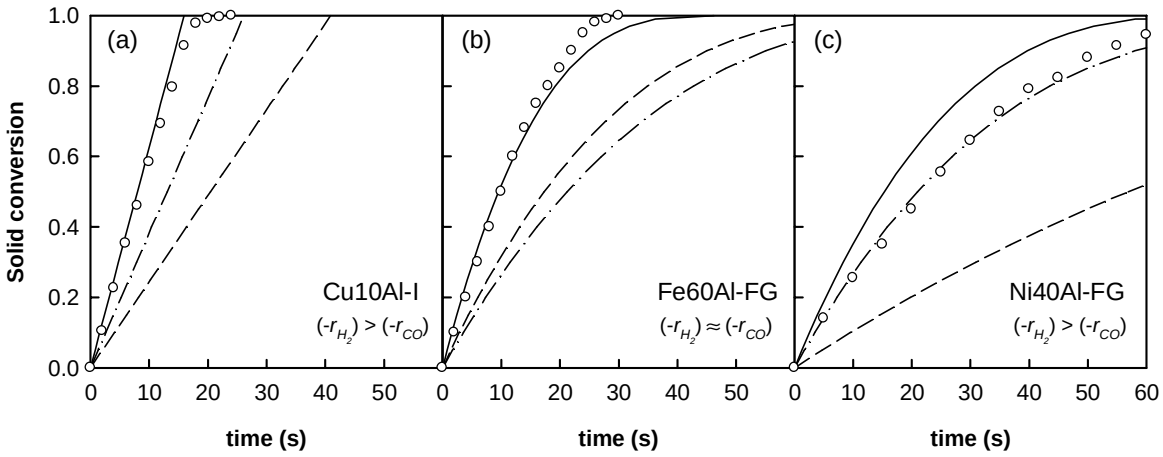

Figure 7. Conversion versus time curves for H_2 and CO mixture. T= 1073 K, P= 2 MPa, gas concentration: 10 vol% H_2 and 10 vol% CO. Experimental data (◦); Model predictions: reaction for H_2 (—·—·–), reaction for CO (– – – –), reaction for H_2 + CO considering the sum of the individual reaction rates (———).

Reduction Kinetics of Cu-, Ni-, and Fe-based Oxygen Carriers Using Syngas ($CO+H_2$) for Chemical-Looping Combustion. Alberto Abad, Francisco García-Labiano, Luis F. de Diego, Pilar Gayán, Juan Adánez

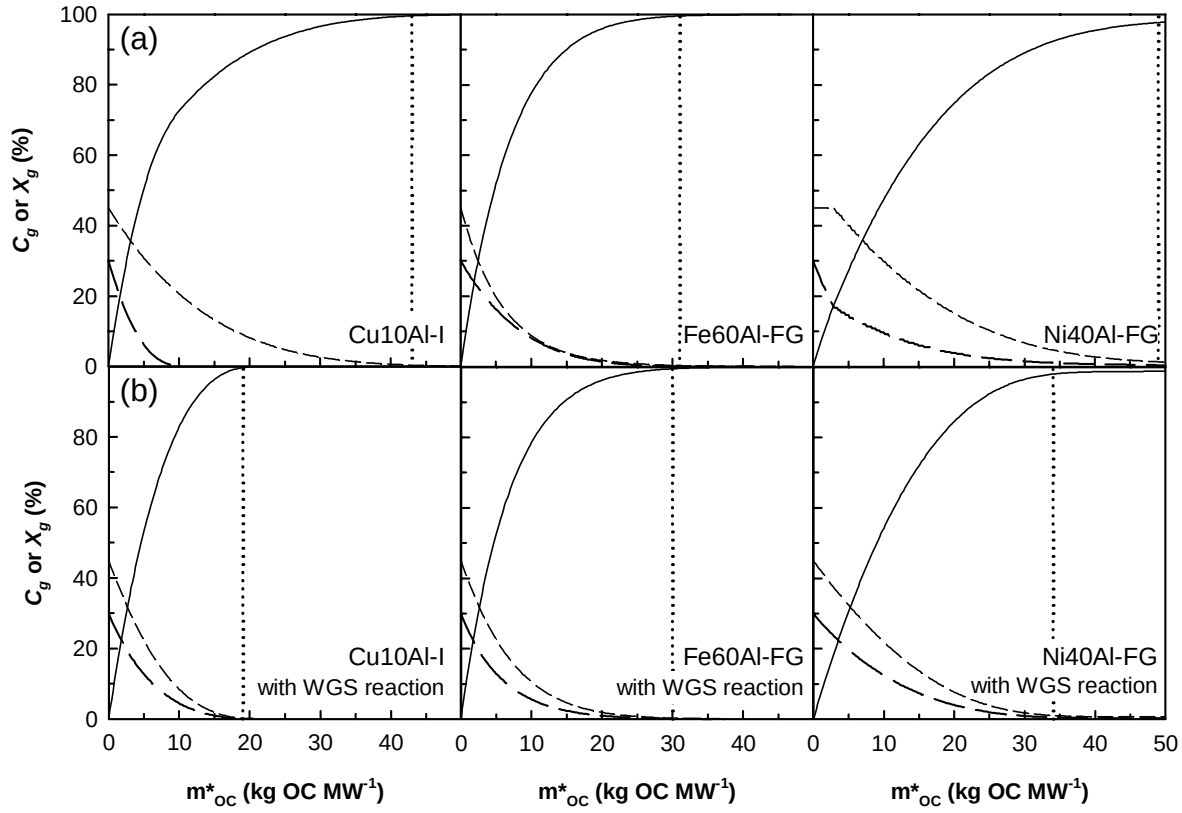

Figure 8. Profiles of H_2 and CO concentration and fuel gas conversion as a function of the mass of oxygen carrier inside the reactor, m^*_{OC}. (a) non-considering the WGS equilibrium; (b) considering the WGS equilibrium. Syngas: 45 vol% CO, 30 vol% H_2, 10 vol% CO_2 and 15 vol% H_2O. 1223 K and 2.0 MPa. Gas concentration: H_2 (—·—·–) and CO (– – – –); Fuel gas conversion (———); solid inventory at X_g = 0.995 for Cu10Al-I and Fe60Al-FG or X_g = 0.98 for Ni40Al-FG (·····)